



## Biological Evaluation and Antioxidant Studies of NiO, PdO and Pt Nanoparticles Synthesized from a New Schiff Base Complexes

**Adnan Abduljabbar Amer**

Department of Chemistry, College of Education  
for Pure Science/ Ibn-Al-Haitham, University of  
Baghdad. Iraq.

[adnanalkaabi12@gmail.com](mailto:adnanalkaabi12@gmail.com)

**Lekaa K. Abdul Kareem**

Department of Chemistry, College of Education  
for Pure Science/ Ibn-Al-Haitham, University of  
Baghdad. Iraq.

[likaa.k.a@ihcoedu.uobaghdad.edu.iq](mailto:likaa.k.a@ihcoedu.uobaghdad.edu.iq)

**Article history: Received 3 June 2022, Accepted 27 June 2022, Published in October 2022.**

**Doi: 10.30526/35.4.2864**

### Abstract

This research included the preparation of Ni, Pd oxide and Pt metal nanoparticles derived from Schiff base (*E*)-2-(((2,5-dichlorophenyl)imino)methyl)-4-methyl phenol octahedral from Ni(II) complex and square planar from Pd(II) and Pt(II) complexes using pulsed laser ablation immersed in deionized water. The optical properties of the prepared NiO, PdO, and Pt nanoparticles were investigated using UV-Visible spectra and FTIR spectrophotometer. The shape and structure were analyzed by Transmission Electron Microscope (TEM) and the X-ray Diffraction Instrument XRD. By using the Scherrer equation, the results showed Ni, Pd, and Pt nanos with average particle sizes of 28.53nm, 20.47nm, and 22.30nm. The biological activity of the nanocomposites was tested against two types of *Escherichia coli*, *Staphylococcus aureus* bacteria, and one type of fungus, such as *candida Albicans*, using antibiotics (Ceftriaxone and metronidazole), showing promising results and the DPPH radical scanning activity is a standard test in studies of antioxidant activity for them.

**Keywords:** Schiff Base, XRD, Nano composites, Antioxidants.

### 1. Introduction

Laser ablation is a type of heating technique where materials such as metal and compounds are melted and evaporated by using a laser beam to generate the nanostructures under a high vacuum system [1,2]. Nowadays, nanotechnology is the first and most important technology because it is a multifunctional technology despite previous scientists have done in their studies, research, and scientific creativity in reducing the size of the particles that make up the material and its impact on the different properties [3-6]. Colloidal copper nanoparticles were prepared by pulsed (Nd:



YAG) laser ablation in water and acetone. The size and optical properties of the nanoparticles were diagnosed by transmission electron microscopy and UV-visible spectrometry. The copper particles were relatively spherical, and their average diameter in water was 30 nm, whereas, in acetone, much smaller particles were produced with an average diameter of 3 nm [7]. Spherical cadmium oxide (CdO) nanoparticles were prepared using pulsed laser ablation (1064 nm, 7 nm, 10 Hz, 80 mJ) from the target cadmium sheets immersed in deionized water. The optical properties of the prepared CdO nanoparticles were investigated by visible spectrophotometer. Ultraviolet shape and structure were analyzed by scanning electron microscopy and transmission electron microscopy[8]. New complexes of cobalt (II), copper (II), nickel (II), manganese (II), and zinc (II) with phthalic anhydride (PL) compounds were synthesized. The prepared complexes were diagnosed using spectroscopic methods. The stability of the complexes on the laser beam was also proven. The results proved that the complexes were stable under the influence of the laser beam used for 10-30 seconds [9]. In this study, the nickel, palladium, and platinum nanoparticles were prepared and diagnosed using the laser ablation method.

## 2.Experimental

### 2.1. Materials and Instruments

Nano of nickel, palladium oxides, and metal platinum were prepared by laser ablation using a pulsed laser type AC220V/50Hz (ND Yag Laser). The chemicals which were used in this study have high purity. The nickel, palladium, and platinum complex disc were pressed under a pressure of 20 Pa to produce a compact disc. The Ultrasonic cell desrupter collected the samples of the nanoscale oxides. Ultra Violet-Visible spectra are performed on a Shimadzu UV- 160A. The FTIR spectra are verified via FTIR - 8400S spectrophotometer on 4000-400 cm<sup>-1</sup>in KBr discs. X-ray diffraction device (XRD) type Expert Phillips Holland. Transmission electron microscope TEM type EM10C, 100 Kv, Germany.

### 2.2. Preparation of Nano oxides

Nickel, palladium, and platinum complexes were prepared from the reaction of the new Schiff base ligand (E)-2-(((2,5-dichlorophenyl)imino)methyl)-4-methyl phenol with the salts of chlorides of the elements as shown in **Figure(1)**. Each of (0.05 g) [Ni(L)2(H<sub>2</sub>O)2], [Pd(L)2] and [Pt(L)2] complexes were pressed under 20 Pa to provide a compact disc. The tablet was then placed in a 100 ml beaker containing deionized water. The sample was irradiated using a pulsed laser device at a dose of 100 mg, 4 Hz, and 300 pulses, and the color was changed to brown. The solution was then collected by filtration, and the supernatant and collected by centrifugation at 14,000 rpm to collect the solid nanoparticles. The concentration of the nanoparticle solution is .0.1 mg/ml.

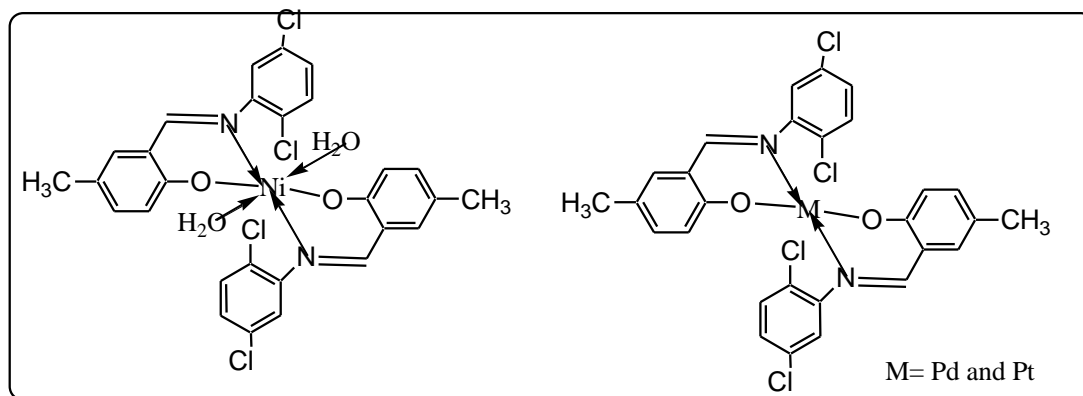


**Figure 1.**The preparation of Schiff base ligand

### 2.3 Biological Activity

The prepared compounds were tested against one type of fungi, such as *Candida Albicans*, and two types of bacteria, such as *Escheria coli* and *Staphylococcus aureus*, by disc diffusion technique. The sample solution was prepared in DMSO as solvent from the concentration of 0.001M. The dishes were brooded for 24 h at room temperature and then the inhibition's diameter was measured and this indicated the growth of bacteria and fungi [10-12].

### 2.4. Antioxidant study

Radical scavenging of 1,1-diphenyl-2-picrylhydrazyl (DPPH).

The assessment of DPPH radical scanning activity is a standard test in antioxidant activity studies. It is a rapid technique to assay the radical scavenging activity of specific compounds [13]. All compounds' free radical scavenging effects and associations were evaluated with DPPH radicals at different concentrations (25, 50, and 100)  $\mu\text{g/ml}$ . After 30 min of incubation in the dark, the absorbance (A) was recorded against a blank at 517 nm using a spectrophotometer (UV-VIS Shimadzu), and IC inhibition of DPPH color values was calculated. DPPH inhibition percentage (Antioxidant Activity %) was calculated using the following formula [14-16]:  $\text{Antioxidant \%} = \frac{A_{\text{blank}} - A_{\text{sample}}}{A_{\text{blank}}} \times 100$ ; where  $A_{\text{blank}}$  is the absorbance of the blank, and  $A_{\text{sample}}$  is the absorbance of the sample. Experiments were duplicated.

## 3. Results and Discussion

### 3.1 FTIR spectrum of Nanoparticles

The infrared spectrum of NiO nanoparticles showed a band at  $1342\text{cm}^{-1}$  belonging to the late CH. It also shows the absorption band at  $829\text{cm}^{-1}$  due to the stretchy vibration of the (C-C) group. The absorption bands at  $\text{cm}^{-1}$  (543-559) belong to the Ni-O bond, which confirms the formation of nickel oxide nanoparticles, NiO NPs, as shown in Figure 2. [17,18]. The infrared spectrum of the palladium oxide nanoparticles, PdO, showed a band at  $438\text{cm}^{-1}$  due to the bending vibration of the lattice CH group. It also shows the absorption band at  $875\text{cm}^{-1}$  due to the stretchy vibration of the (C-C) group, and the absorption band at  $617\text{cm}^{-1}$  and this indicated the presence of a Pd-O bond, as shown in Figure 3. The infrared spectrum of the platinum metal nanoparticles (Pt) showed a band in the range of ( $2924\text{-}2850\text{cm}^{-1}$ ) and  $1338\text{cm}^{-1}$  and this due to the stretchable and flexural vibration of the CH group  $1438\text{cm}^{-1}$  alpha. ) as shown in **Figure 4** [19, 20].

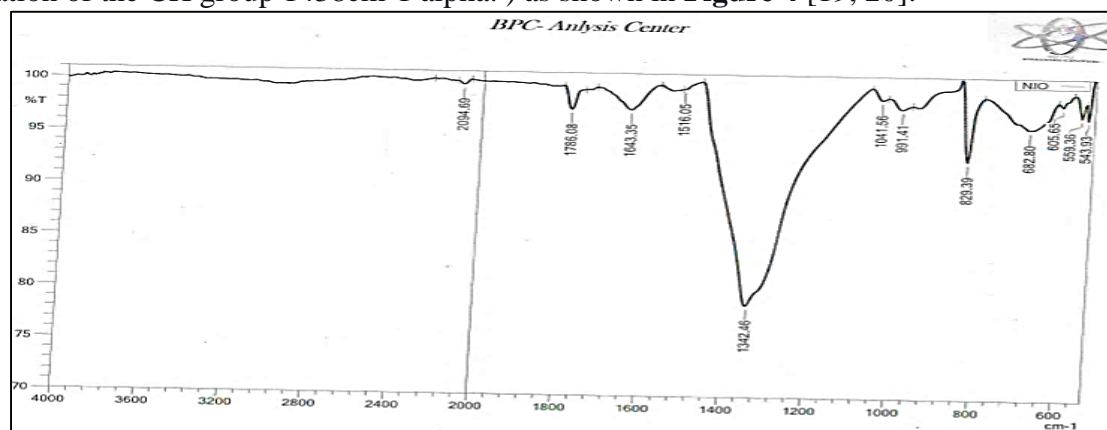


**Figure 2.** FT-IR spectrum of NiO NPs

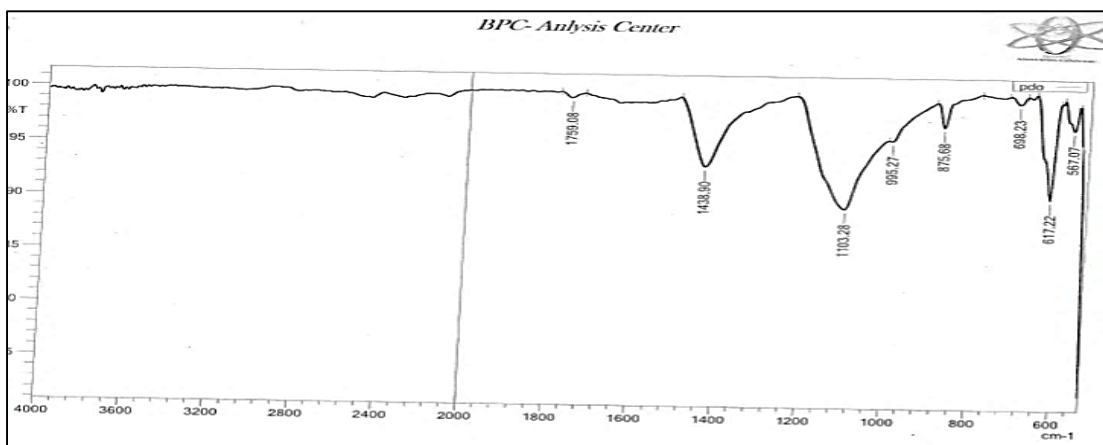


**Figure 3.** FT-IR spectrum of PdO NPs

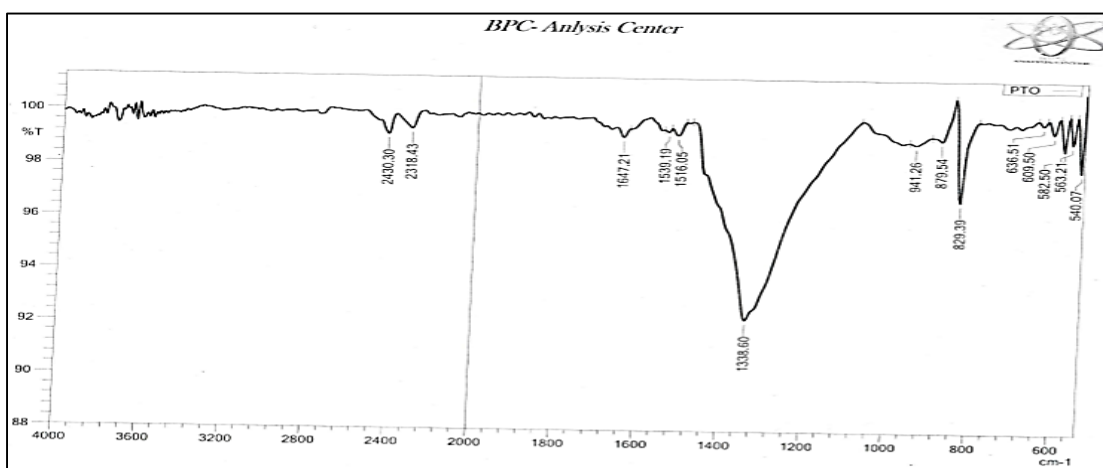


**Figure 4.** FT-IR spectrum of Pt NPs

### 3.2. UV-Visible Spectra

The ultraviolet spectrum of the nickel oxide and palladium nanoparticles showed absorption peaks at (230 nm and 204) due to the  $\pi-\pi^*$  electron transition and (266,300,386) nm to the  $\pi-\pi^*$  electron transition and the charge transfer spectrum, which indicates the formation of nickel oxide and palladium oxide nanoparticles, respectively, as in Figures (5 and 6). This agrees with what was stated in the previous literature [21,22]. As for the UV-Visible spectrum of the platinum nano-metal in **Figure 7**, it showed an absorption peak at 268 nm due to the electronic

transition of  $\pi-\pi^*$ , which is consistent with what was stated in the literature [23].

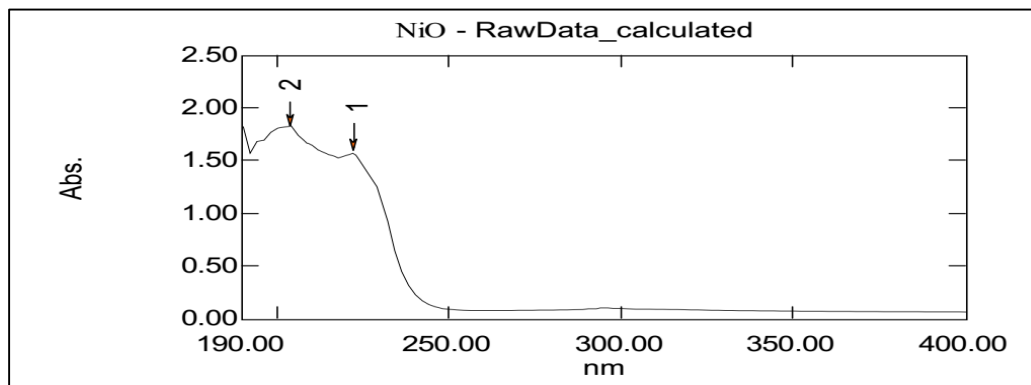


Figure 5. UV spectrum of nickel oxide nanoparticles

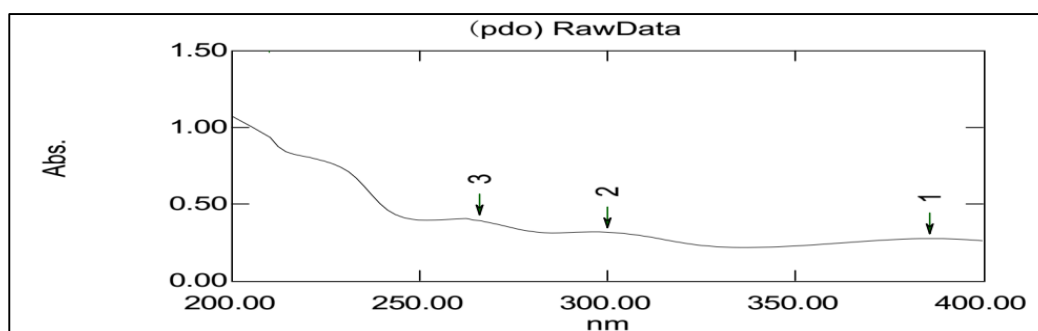


Figure 6. UV spectrum of palladium oxide nanoparticles

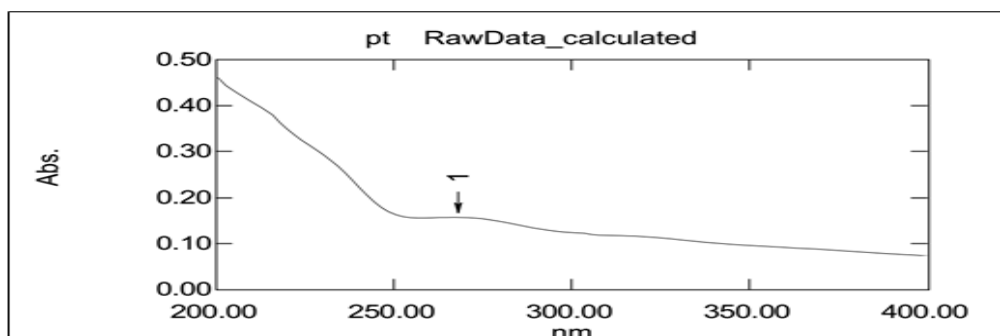
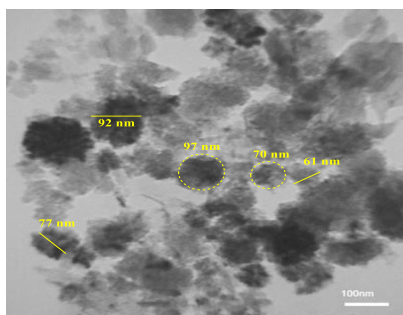


Figure 7. UV spectrum of the platinum nano metal

### 3.3. Transmission Electron Microscope (TEM)

The transmission electron microscope is one of the techniques that are adopted to reach a high-resolution image of materials at the nano scale, as the measurement of the electron beam inside the sample to be examined is known. The TEM measurement in **Figure (8)** of nickel oxide showed the presence of ball-like structures whose size ranges between 70 nm and 97 nm in addition to irregular shaped structures whose sizes ranged from 61 nm to 92 nm. The distribution of nanoparticles in **Figure (9)** proved that the distribution was within the range of 40-90 nm. **Figure (10)** showed the presence of regular geometric structures similar to balls with sizes 13-18 nm in addition to regular geometric structures similar to rectangles with dimensions of 22 \* 13 and 15 \* 10 nm. The distribution of nanoparticles in **Figure (11)** proved that the distribution was within the range of 2-22 nm. It is characteristic that the resulting structures had rough surfaces, which indicates that the result of aggregates of nanoparticles smaller than nickel oxide. This is evidence of the successful formation of nickel oxide nanoparticles from its complexes. The measurement contains most of the areas in the form of light areas, which indicates that the nanoparticles of nickel

oxide do not accumulate, and this is due to the presence of ligands that act as inhibitors of particles gathering [24].



**Figure 8.** TEM measurement of spherical and irregularly shaped NiO NPs

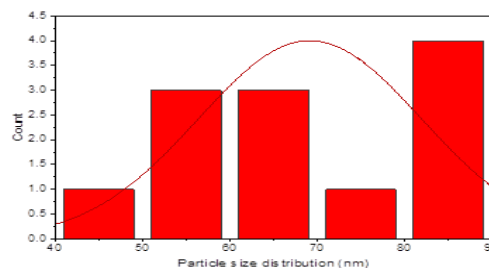


**Figure 9.** TEM measurement of spherical and irregularly shaped NiO NPs

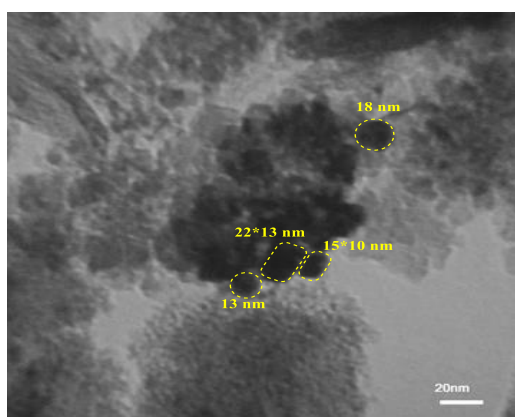


**Figure 9.** TEM measurement of spherical and rectangular NiO NPs

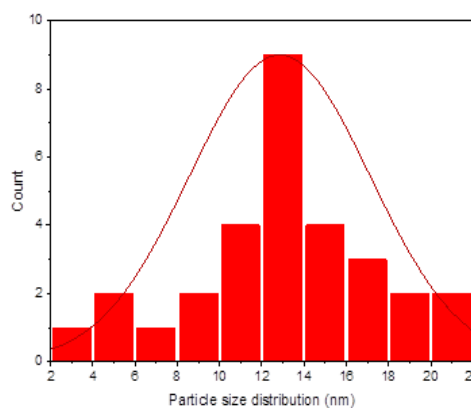


**Figure 11.** Distribution of spherical and irregular NiO NPs

The TEM measurement in **Figure (12)** of palladium oxide showed the presence of a tubular structure with a length not exceeding 720 nm and a diameter not exceeding 85 nm. Figure (13) shows the surface of this tube, which contains semi-regular spherical structures with a diameter within the range of 4-19 nm. The distribution of nanoparticles in **Figure (14)** proved that the distribution was within the range of 2-18 nm. The presence of these small particles confirms that the tubes are composed of smaller nanoparticles lined up next to each other to form palladium oxide nanotubes [25].

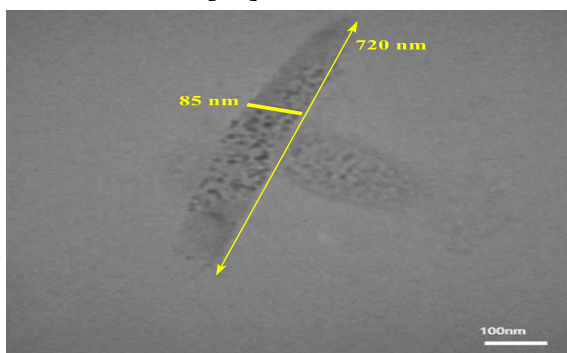


**Figure 12.** TEM measurement of PdO nanotubes

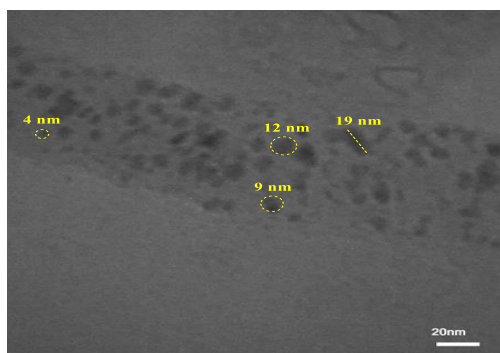


**Figure 13.** TEM measurement of the surface of PdO nanotubes

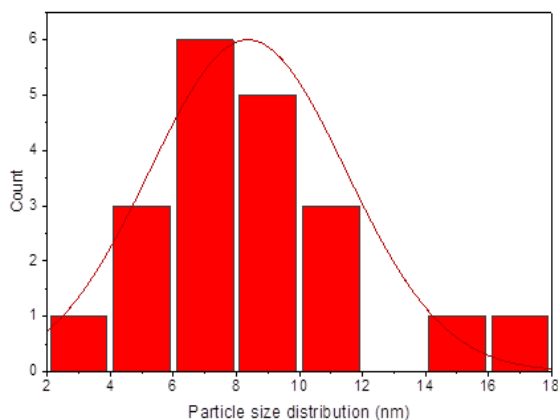


**Figure 14.** Distribution of spherical palladium oxide nanoparticles on the surface of a palladium nanotube

In **Figure (15)**, the TEM measurement of platinum nanoparticles was found in the form of hexagons of platinum nanoparticles, with a side length of approximately 38-40 nm, a width of 69 nm, and a length of 77 nm. The measurement also showed that the nano-platinum might be in the form of long, irregular chains with a diameter within the range of 65-12 nm, as shown in **Figures (16 and 17)** [26].

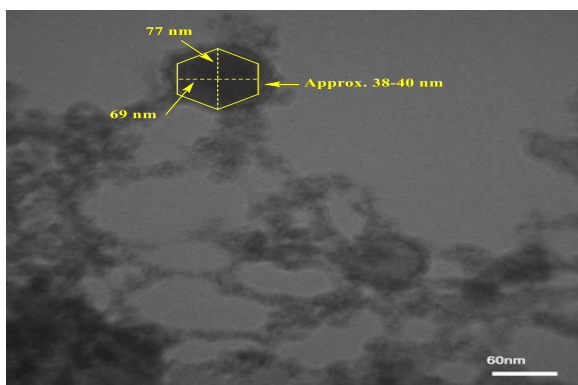


**Figure 15.** TEM measurement of platinum hexagons

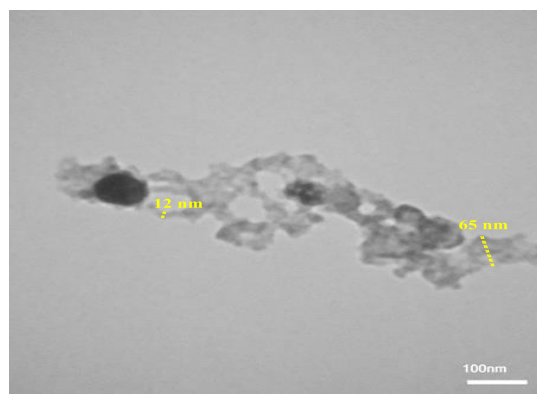


**Figure 16.** TEM measurement of platinum Nano chains

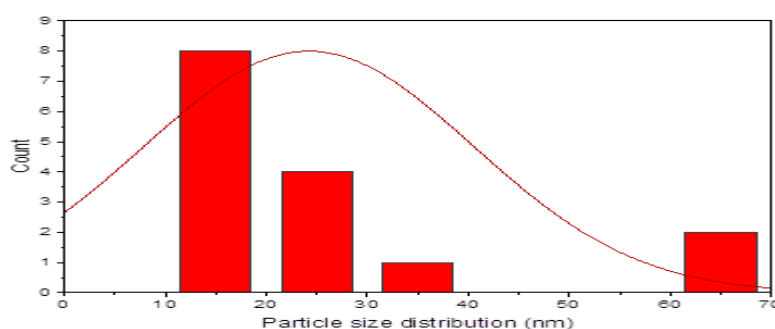


**Figure 17.** Distribution of platinum nano-chains

### 3.4. The X-ray diffraction

The X-ray diffraction measurement in **Figure (18)** showed the presence of the main peaks of nickel oxide, which appeared at 37.4014, 43.5194, 63.0645, 75.8147, and 77.7895 degrees, with FWHM values of 0.2952, 0.3444, 0.1968, 0.6888 and 0.4800 degrees, which correspond to Miller's coefficients. The following are: 111, 200, 220, 311, and 222 which correspond to JCPDS 47-1049 [27]. The size of the nickel oxide nanoparticles was calculated using the Scherrer equation, and it

was found that the average size was 28.53 nm. This size greatly agrees with the sizes of nickel oxide nanospheres and rectangles determined by the TEM technique, as shown in **Table (1)**. The measurement also shows the presence of other peaks, which can be attributed to the ligand or complex residue surrounding the nickel oxide nanoparticles.

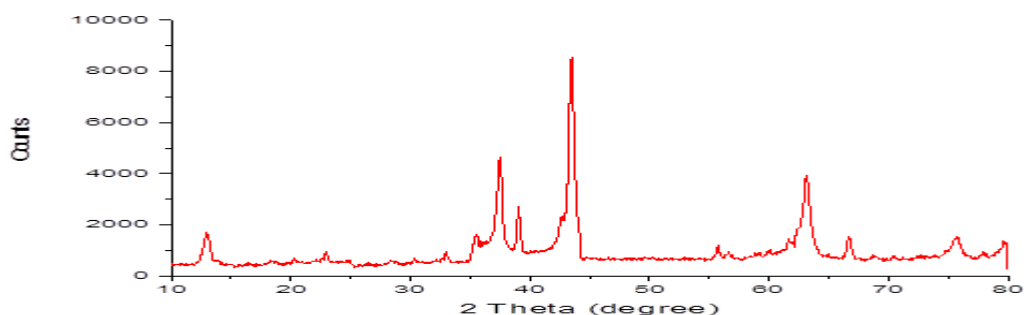


**Figure 18.** X-ray diffraction of NiO NPs

**Table 1.** X-ray diffraction information for NiO NPs and average particle size calculated by Scherrer equation

Pos. [ $^{\circ}2\text{Th.}$ ]	Height [cts]	FWHM [ $^{\circ}2\text{Th.}$ ]	Particle size (nm)	Average particle size (nm)
37.4014	3913.45	0.2952	29.70	28.53
43.5194	8132.74	0.3444	25.96	
63.0645	3409.23	0.1968	49.50	
75.8147	1029.25	0.6888	15.28	
77.7895	416.53	0.4800	22.23	

The X-ray diffraction measurement in **Figure (19)** showed the presence of the main peaks of palladium oxide, which appeared at 33.2, 42.3, 53.8, 62.5, and 70.1 degrees, with FWHM values of 0.63725, 0.43585, 0.977, 0.53279 and 0.25 degrees which correspond to the following Miller's coefficients: 101, 110, 112, 103, and 202, respectively, which corresponds to JCPDF 85-0624 [28]. The measurement also indicated the presence of other peaks, which can be attributed to the ligand or complex residues surrounding the palladium oxide nanoparticles. The size of the palladium oxide nanoparticles was calculated using the Scherrer equation, and it was found that the average size was 20.47 nm. This size is in great agreement with the sizes of the palladium oxide nanospheres found on the surface of the palladium oxide nanotubes determined by TEM technology, as shown in **Table (2)**.

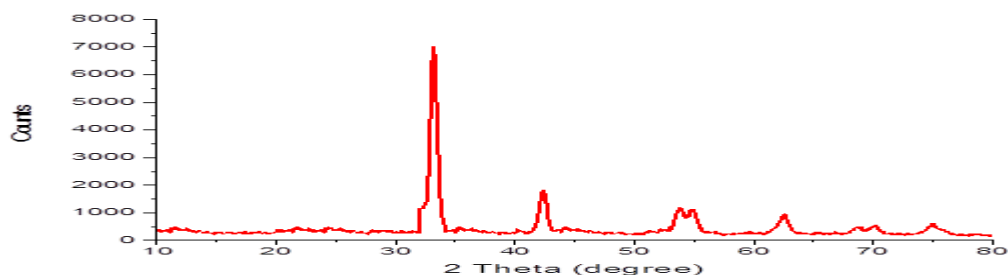


**Figure 19.** X-ray diffraction of Nano scale PdO NPs

**Table 2.** X-ray diffraction information for PdO NPs and average particle size calculated by Scherrer equation

Pos. [°2Th.]	Height [cts]	FWHM [°2Th.]	Particle size (nm)	Average particle size (nm)
33.2	6875.4	0.63725	13.60	20.47
42.3	1691.2	0.43585	20.43	
53.8	1052.8	0.977	9.53	
62.5	814.8	0.53279	18.23	
70.1	408.8	0.25	40.57	

The X-ray diffraction measurement in **Figure (20)** showed the presence of the main peaks of platinum metal, which appeared at 39.8066, 47.7100, and 66.4561 degrees, with FWHM values of 0.41104, 0.39437, and 0.44325 degrees, which correspond to the following Miller's coefficients: 111, 200 and 220, respectively which corresponds to JCPDF 4-802 [29]. The measurement also indicated the presence of other peaks, which can be attributed to the ligand or complex residues surrounding the alilatin nanometal. The size of platinum nanoparticles was calculated using the Scherrer equation, and it was found that the average size was 22.30 nm. This size is in great agreement with the sizes of the specific platinum nano-chains determined by TEM technology, as shown in **Table (3)**. The measurement also showed the presence of other peaks, which can be attributed to the ligand or complex residues surrounding the alilatin nanometal.

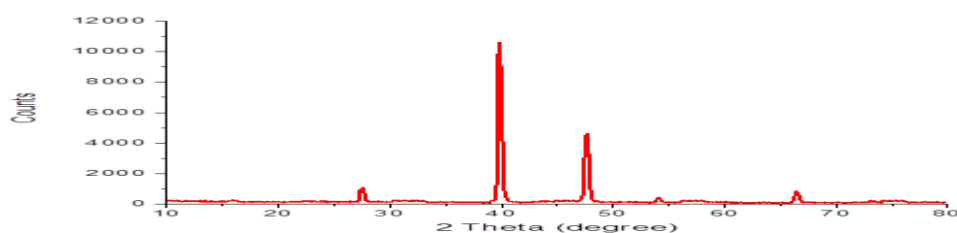


**Figure 20.** X-ray diffraction of a Pt NPs

**Table 3.** X-ray diffraction information for Pt NPs and average particle size calculated by Scherrer equation

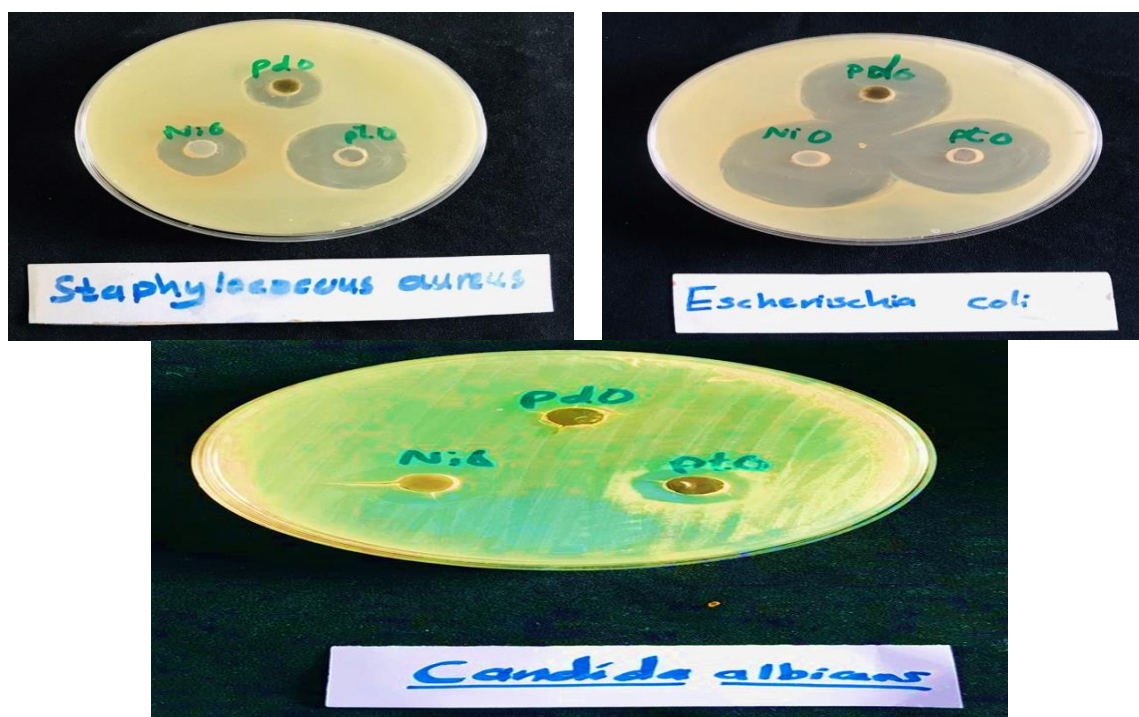
Pos. [°2Th.]	Height [cts]	FWHM [°2Th.]	Particle size (nm)	Average particle size (nm)
39.8066	10530.12	0.41104	21.49	22.30
47.7100	4497.69	0.39437	23.02	
66.4561	673.38	0.44325	22.40	

### 3.5. Biological Activity Study

The biological activity of the prepared new NiO, PdO, and Pt was studied against the selected type of microorganisms. It included gram-positive bacteria such as *staphylococcus aureus* and gram-negative bacteria, such as *E.coli*, in the agar diffusion method, which is used (DMSO) as a solvent. The nanocomposites showed a good activity against two types of positive and negative bacteria and one type of candida Albicans, as shown in **Table (4)** and **Figure (21)** [30].

**Table 4.** Diameter of the antibiotic inhibition circuit for Nano composites

Compounds	<i>Escherichia coli</i>	<i>Staphylococcus aureus</i>	<i>candida albicans</i>
<i>Ceftriaxone</i>	35	30	0
<i>Metronidazole</i>	0	0	15
NiO NPs	39	20	17
PdO NPs	32	18	12
Pt NPs	33	27	15

**Figure 21.** The inhibition diameter of oxides (nickel and palladium) and nano platinum for two types of bacteria and one type of fungi.

### 3.6. The Study of Antioxidants

The DPPH method was used as the Schiff base ligand's antioxidant activity, the prepared complexes, the oxides (nickel and palladium), and platinum nanoparticles free radicals [31]. The percentage of antioxidant activity of the ligand and some of the prepared complexes were evaluated by scavenging the free radicals of the DPPH molecule according to the following equation:

The results showed that the color of the DPPH solution changed from purple to light yellow due to the dissolution of free radicals by ligands and complexes, donating hydrogen to form a stable molecule DPPH-H. This means that it possesses antioxidant activity because it contains the proton that can give it to scavenge free radicals. Then it can use it to inhibit the growth of cancer cells, as the ligand and its complexes were able to scavenge the free radical on the DPPH molecule by donating one of the protons in the ligand or complexes.

$$\text{Scavenger Activity \%} = 100 - (A_0 - A_t / A_0) * 100$$

Where A<sub>0</sub> is the absorbance of DPPH, it represents the absorbance of the extracted solution with DPPH. As for the effectiveness of nickel and palladium oxide particles and platinum nanoparticles, IC<sub>50</sub> cannot be estimated because the higher concentration and the lower the effectiveness [32].

**Table 5.** The percentage of free radical scavenging or the percentage of antioxidants for a period of 30 min

9+9+99+	conc. µg			IC50
	25	50	100	
Tested with DPPH				
Vit.C	89.16	93.68	95.68	14
NiO NPs	19.08	18.09	17.03	---
PdO NPs	16.82	14.55	8.76	---
Pt NPs	19.78	13.99	11.08	---

#### 4. Conclusion

NiO, PdO, and Pt nanos, with average particle sizes of 28.53nm, 20.47, and 22.30, respectively, were successfully synthesized by laser ablation in a liquid environment. The optical characterization was studied using UV-VIS spectrophotometer and FT-IR. The material structure was investigated using XRD, and the morphological properties were studied using TEM techniques. The experimental results of XRD and FT-IR analyses confirmed the formation of NiO, PdO, and Pt nanos phases.

#### References

1. Goutam, S. P.; Saxena, G.; Roy, D.; Yadav, A. K.; Bharagava, R. N.. Green synthesis of nanoparticles and their applications in water and wastewater treatment. *In Bioremediation of industrial waste for environmental safety*, Springer, Singapore. **2020**: 349-379.
2. Amendola, V.; Meneghetti, M. What controls the composition and the structure of nanomaterials generated by laser ablation in liquid solution?. *Physical Chemistry Chemical Physics*. **2013**,15(9): 3027-3046.
3. Anastas, P.; Eghbali, N. Green chemistry: principles and practice. *Chemical Society Reviews*. **2010**, 39(1): 301-312.
4. Mafuné, F.; Kohno, J. Y.; Takeda, Y.; Kondow, T.; Sawabe, H. Formation of gold nanoparticles by laser ablation in aqueous solution of surfactant. *The Journal of Physical Chemistry B*, **2001**. 105(22): 5114-5120.
5. Rao, S. V.; Podagatlapalli, G. K.; Hamad, S. Ultrafast laser ablation in liquids for nanomaterials and applications. *Journal of nanoscience and nanotechnology*.**2014**, 14(2): 1364-1388.
6. Tsuji, T.; Thang, D. H.; Okazaki, Y.; Nakanishi, M.; Tsuboi, Y.; Tsuji, M. Preparation of silver nanoparticles by laser ablation in polyvinylpyrrolidone solutions. *Applied Surface Science*. **2008**, 254(16): 5224-5230.
7. Tilaki, R. M.; Mahdavi, S. M. Size, composition and optical properties of copper nanoparticles prepared by laser ablation in liquids. *Applied Physics A*. **2007**, 88(2): 415-419.

8. Mostafa, A. M.; Yousef, S. A.; Eisa, W. H., Ewaida, M. A.; Al-Ashkar, E. A. Synthesis of cadmium oxide nanoparticles by pulsed laser ablation in liquid environment. *Optik*. **2017**,*144*: 679-684.
9. Salih, B. D.; Dalaf, A. H.; Alheety, M. A.; Rashed, W. M.; Abdullah, I. Q. Biological activity and laser efficacy of new Co (II), Ni (II), Cu (II), Mn (II) and Zn (II) complexes with phthalic anhydride. *Materials Today: Proceedings*. **2021**, *43*: 869-874.
10. Tweedy B., *Phytopathology*, **1964**,*55*: 910- 914.
11. Srivastava, K. P.; Sunil Kumar Singh; Bir Prakash M., *Journal of Chemical and Pharmaceutical Research*. **2015**, (7):197-203.
12. Abdel-Rahman, L. H.; Abu-Dief, A. M.; Moustafa, H.; Abdel-Mawgoud, A. A. H. Design and nonlinear optical properties (NLO) using DFT approach of new Cr (III), VO (II), and Ni (II) chelates incorporating tri-dentate imine ligand for DNA interaction, antimicrobial, anticancer activities and molecular docking studies. *Arabian Journal of Chemistry*. **2020**, *13(1)*: 649-670.
13. Olszowy, M.; Dawidowicz, A. L. Is it possible to use the DPPH and ABTS methods for reliable estimation of antioxidant power of colored compounds?. *Chemical Papers*. **2018**, *72(2)*: 393-400.
14. AlSaady, T. A.; Madlum, K. N.; Obied, H. N. Effect of antioxidants on cisplatin-induced cytotoxicity and oxidative stress in colon cancer cells. *EurAsian Journal of BioSciences*. **2020**,*14(2)*.
15. El Malah, T.; Nour, H. F.; Satti, A. A.; Hemdan, B. A.; El-Sayed, W. A. Design, synthesis, and antimicrobial activities of 1, 2, 3-triazole glycoside clickamers. *Molecules*. **2020**, *25(4)*: 790.
16. Kareem, M. J.; Al-Hamdani, A. A. S.; Jirjees, V. Y.; Khan, M. E.; Allaf, A. W.; Al Zoubi, W. Preparation, spectroscopic study of Schiff base derived from dopamine and metal Ni (II), Pd (II), and Pt (IV) complexes, and activity determination as antioxidants. *Journal of Physical Organic Chemistry*. **2021**, *34(3)*: e4156.
17. Prabhu, S.;Thangadurai, T. D.; Bharathy, P. V.; & Kalugasalam, P. Synthesis and characterization of nickel oxide nanoparticles using Clitoria ternatea flower extract: Photocatalytic dye degradation under sunlight and antibacterial activity applications. *Results in Chemistry*. **2022**, *4*: 100285.
18. Refat, M. S.; Saad, H. A.; Gobouri, A. A.; Alsawat, M.; Belgacem, K.; Majrashi, B. M.; Adam, A. M. A. Synthesis, characterization, and photocatalytic efficiency of a new smart PdO oxide nano materials for using in the recycling and sustainable wastewater treatment. *Bulletin of the Chemical Society of Ethiopia*. **2021** ,*35(1)*:107-118.
19. Al-Obidi, L. K.; T. H. Al-Noor., Synthesis, Spectral and Bacterial Studies of Mixed Ligand Complexes of Schiff Base Derived from Methyl-dopa and Anthranilic Acid with Some Metal Ions. *Ibn AL-Haitham Journal for Pure and Applied Science*. **2018**, 235-247.
20. Naji, Shaymaa H.; Lekaa K. Abdul Karim; Falih H. Mousa. Synthesis, Spectroscopic and Biological Studies of a New Some Complexes with N-Pyridin-2-Ylmethyl-Benzene-1, 2Diamine. *Ibn AL-Haitham Journal for Pure and Applied Science*. **2017**, *26.1*: 193-207.
21. Sabouri, Z.; Akbari, A.; Hosseini, H. A.; Khatami, M.; Darroudi, M. Green-based bio-synthesis of nickel oxide nanoparticles in Arabic gum and examination of their cytotoxicity, photocatalytic and antibacterial effects. *Green Chemistry Letters and Reviews*. **2021** ,*14(2)*: 404-414.

22. Refat, M. S.; Saad, H. A.; Gobouri, A. A.; Alsawat, M.; Belgacem, K.; Majrashi, B. M.; Adam, A. M. A. Synthesis, characterization, and photocatalytic efficiency of new smart PdO oxide nanomaterials for using in the recycling and sustainable wastewater treatment. *Bulletin of the Chemical Society of Ethiopia*. **2021**, *35(1)*:107-118.
23. Poddar, A. K.; Patel, S. S.; Patel, H. D. Synthesis, characterization and applications of conductive polymers: A brief review. *Polymers for Advanced Technologies*. **2021**, *32(12)*: 4616-4641.
24. Alheety, M. A.; Al-Jibori, S. A.; Ali, A. H.; Mahmood, A. R.; Akbaş, H., Karadağ, A.; Ahmed, M. H. Ag (I)-benzisothiazolinone complex: synthesis, characterization, H<sub>2</sub> storage ability, nano transformation to different Ag nanostructures and Ag nanoflakes antimicrobial activity. *Materials Research Express*. **2019**, *6(12)*: 125071.
25. Vinodhini, S.; Vithiya, B. S. M.; Prasad, T. A. A. Green synthesis of palladium nanoparticles using aqueous plant extracts and its biomedical applications. *Journal of King Saud University-Science*. **2022**,*34(4)*: 102017.
26. Mahajan, A.; Deshpande, P.; Butee, S. Synthesis and characterization of NiO/ZnO composite prepared by solid-state reaction method. *Materials Today: Proceedings*. **2022**,*50*: 1912-1917.
27. Yan, H.; Zhang, D.; Xu, J.; Lu, Y.; Liu, Y.; Qiu, K.; Luo, Y. Solution growth of NiO nanosheets supported on Ni foam as high-performance electrodes for supercapacitors. *Nanoscale research letters*. **2014**, *9(1)*: 1-7.
28. Gao, S.; Hu, S.; Luo, G.; Sun, S.; Zhang, X. 2, 2'-bipyridine palladium (II) complexes derived N-doped carbon encapsulated palladium nanoparticles for formic acid oxidation. *Electrochimica Acta*. **2022**, *413*: 140179.
29. Eltaweil, A. S.; Fawzy, M.; Hosny, M.; Abd El-Monaem, E. M.; Tamer, T. M.; Omer, A. M. Green synthesis of platinum nanoparticles using Atriplex halimus leaves for potential antimicrobial, antioxidant, and catalytic applications. *Arabian Journal of Chemistry*. **2022**,*15(1)*: 103517.
30. Al-Zinke, J. M. M.; Jarad, A. J. Synthesis, spectral studies and microbial evaluation of azo dye ligand complexes with some transition metals. *Journal of Pharmaceutical Sciences and Research*. **2019**, *11(1)*: 98-103.
31. Al-Hamdani, A. A. S.; BALKHI, A., Falah, A.; Shaker, S. A. New Azo-Schiff base derived with Ni (II), Co (II), Cu (II), Pd (II) and Pt (II) Complexes: Preparation, spectroscopic investigation, structural studies and biological activity. *Journal of the Chilean Chemical Society*. **2015**, *60(1)*: 2774-2785.
32. Al-Haidari, A. S.; Al-Tamimi, E. O. Synthesis of new 5-aryl tetrazoline and evaluation of their antifungal and antibacterial activity. *Egyptian Journal of Chemistry*. **2021**, *64(10)*: 3-4.